INL/CON-25-83146-Revision-0

FIDES-II/P2M Simulation Exercise on AN3 and AN10 bump tests: main results

October 2025

J. Sercombe, A. Vernier, V. D'Ambrosi, I. Gunot-Delahaie, S. Bjaoui, D. Rozzia, G. Bonny, B. Boer, A. Ambard, A. Mohamad, Y. Udagawa, J. Corson, A. Scheuermann, K. A. Gamble, R. J. Armstrong, L.-E. Herranz, C. Aguado, F. Feria, A. Toptan, Y. Long

Changing the World's Energy Future

Idaho National Laboratory

INL is a U.S. Department of Energy National Laboratory operated by Battelle Energy Alliance, LLC

INL/CON-25-83146-Revision-0

FIDES-II/P2M Simulation Exercise on AN3 and AN10 bump tests: main results

J. Sercombe, A. Vernier, V. D'Ambrosi, I. Gunot-Delahaie, S. Bjaoui, D. Rozzia, G. Bonny, B. Boer, A. Ambard, A. Mohamad, Y. Udagawa, J. Corson, A. Scheuermann, K. A. Gamble, R. J. Armstrong, L.-E. Herranz, C. Aguado, F. Feria, A. Toptan, Y. Long

October 2025

Idaho National Laboratory
Idaho Falls, Idaho 83415

http://www.inl.gov

Prepared for the
U.S. Department of Energy
Under DOE Idaho Operations Office
Contract DE-AC07-05ID14517

FIDES-II/P2M Simulation Exercise on AN3 and AN10 bump tests: main results.

J. Sercombe[1*], A. Vernier[1], V. D'Ambrosi[1], I. Guénot-Delahaie[1], S. Béjaoui[1], D. Rozzia[2], G. Bonny[2], B. Boer[2], R.-W. Bosch[2], A. Ambard[3], A. Chaieb[3], A. Mohamad[4], Y. Udagawa[4], J. Corson[5], A. Scheuermann[5], K.A. Gamble[6], R. Armstrong[6], L.-E. Herranz[7], C. Aguado[7], F. Feria[7], A. Toptan[8], Y. Long[8]

[1]CEA, DES, IRESNE, DEC, Cadarache, F-13108 Saint-Paul-lez-Durance, France; [2]Belgian Nuclear Research Centre (SCK CEN), Mol, Belgium; [3]EDF R&D, Avenue des Renardières, Ecuelles, 77818 Moret-sur-Loing Cedex, France; [4]Japan Atomic Energy Agency Tokai-mura, Naka-gun, 319-1195 Ibaraki, Japan; [5]U.S. Nuclear Regulatory Commission, Washington, DC 20555-0001, USA; [6]Idaho National Laboratory, P.O. Box 1625, Idaho Falls, ID 83415, USA; [7]Centro de Investigaciones Energeticas, Medioambientales y Tecnologicas (CIEMAT), 28040 Madrid, Spain; [8]Westinghouse Electric, Cranberry Township, Pennsylvania, USA.

ABSTRACT

This paper presents simulations of bump tests conducted as part of the P2M (Power to Melt and Maneuverability) project within the OECD/NEA FIDES-II framework (Framework for Irradiation Experiments). To prepare fuel performance codes for analyzing the P2M experiments, an international Simulation Exercise (SE) was initiated under the P2M project. The objective of this exercise was to model the AN3 and AN10 bump tests carried out in the 1980s at the DR3 reactor (3rd RISØ Fission Gas Project), during which instrumented fuel rodlets (equipped with thermocouples and pressure sensors) were subjected to prolonged power transients and power dips. The ongoing simulation exercise involves seven organizations from industry, research, and regulatory bodies, each using different fuel performance codes. This paper provides detailed descriptions of the test cases and simulation results from six fuel performance codes (ALCYONE, BISON, FAST, FEMAXI, FRAPCON, and TRANSURANUS), with a particular focus on fission gas release kinetics.

Keywords: P2M, simulation, fuel performance code, fission gas release, burst release

1. INTRODUCTION

The Power to Melt and Maneuverability (P2M) Joint Experimental Program (JEEP) is one of the experimental initiatives within the OECD/NEA FIDES-II framework [1] (Framework for Irradiation Experiments), led by the core group consisting of CEA, EDF, and SCK CEN. The program aims to conduct ramp tests on modern high-burnup fuel rods in the BR2 reactor at SCK CEN, with the goal of inducing incipient melting of the fuel core [2] (up to a maximum of 10% volume at the Peak Power Node). The test rods will be instrumented with a centerline thermocouple and a pressure sensor in the plenum [3].

To assess the behavior of the instrumentation before conducting the power-to-melt experiments, the second P2M test (P2M-Q1) will involve irradiating a high-burnup fuel rod (74 GWd/tU) for 30 days, with an average (maximum) Linear Heat Rate (LHR) of 250 (300) W/cm. The pre-design of this test is based heavily on fuel performance simulations conducted by the core group using ALCYONE [4] (CEA), TRANSURANUS [5] (SCK CEN), and CYRANO3 [6] (EDF). To prepare the fuel performance codes, past experiments featuring online measurements of plenum pressure and fuel pellet temperature (the AN3 and

AN10 bump tests [7]) were selected, and the simulations were made open to FIDES-II members. Seven participants from five countries, using six different fuel performance codes, joined the Simulation Exercise (SE).

This paper begins by presenting the test cases AN3 and AN10, along with a review of the simulations previously conducted by various teams prior to this SE. Section 3 provides a detailed description of the key features of the fuel performance codes in relation to the objectives of this SE. The simulation results are presented in Section 4, focusing on temperature, plenum pressure, and fission gas release (FGR) measurements. Three-dimensional simulations conducted with ALCYONE, aimed at more accurately capturing the reopening of the pellet-clad gap, are then discussed in detail. Finally, conclusions are drawn from the SE, highlighting the lessons learned for the P2M-Q1 test design.

2. AN3 AND AN10 BUMP TESTS

The AN3 and AN10 bump tests were conducted in the late 1980s at the DR3 experimental reactor in Risø, Denmark, as part of the Third Risø Fission Gas Program [7]. These tests were carried out on rod segments composed of UO_2 with Zy-4 cladding and a bonded Zr liner. The rods had been pre-irradiated over four cycles in the Biblis A PWR, reaching an average burnup of 36 GWd/tU. AN3 and AN10 were chosen for their relevance to the upcoming P2M-Q1 test, particularly because both included online measurements of temperature and pressure. AN3, in particular, has been the subject of numerous simulation studies, as elaborated in the following paragraph. The AN3 test followed a staircase power ramp, peaking at an average Linear Heat Rate (LHR) of 407 W/cm, which was sustained for approximately two days. AN10 reached a slightly lower average LHR of 344 W/cm, also maintained for two days, following a brief conditioning phase at 200 W/cm. This makes AN10 more representative of the expected LHR conditions for P2M-Q1. Both tests included two power dips to 200 W/cm—one at the midpoint of the holding period and another just before shutdown. The ramp rates throughout the tests remained below 60 W/cm/min. Figure 1 illustrates the rod's average power histories for AN3 and AN10, along with the corresponding pressure sensor readings and estimated Fission Gas Release (FGR).

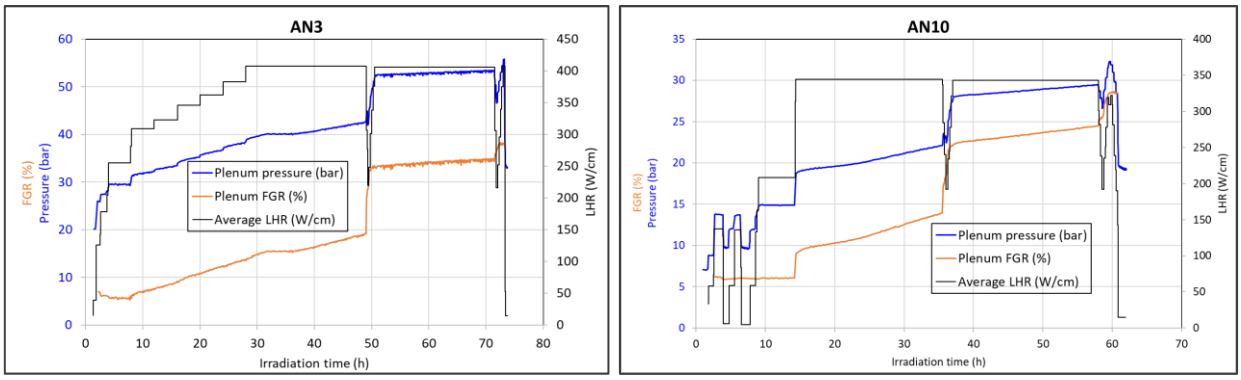

Figure 1. Average LHR, pressure measurements and estimated FGR during the AN3 and AN10 bump tests.

One of the key features of the AN3 bump test that has attracted significant modeling interest is the observed pressure increase and distinct Fission Gas Release (FGR) steps during the power dips—an effect that standard fission gas models often struggle to reproduce. In 1999, Koo et al. introduced a simple burnup- and LHR-dependent criterion in the COSMOS code to account for these FGR steps during AN3 [8]. The International Atomic Energy Agency's FUel Modeling at EXtended Burnup II (FUMEX-II) project, conducted between 2002 and 2007, also focused on the AN3 bump test [9]. It attributed the pronounced FGR step during the power dip to a possible mechanical hold-up of fission gas in the fuel-cladding gap,

which could have connected to the plenum only during the power reduction. More recently, Pizzocri et al. proposed a model linking fuel pellet temperature variations and burnup to micro-cracking at grain faces during both power increases and decreases in ramp tests [10]. This model, implemented in the zero-dimensional SCIANTIX fission gas solver, has been applied in the TRANSURANUS and BISON codes, yielding consistent predictions of FGR behavior during AN3 [11], and more recently in the OFFBEAT [12] and FRAPCON [13] codes. In 2024, Khvostov introduced a delayed axial redistribution mechanism for released fission gases in the FALCON code to explain the substantial FGR step observed during the power dip of the AN3 test [14].

3. PARTICIPANTS AND CODES

Table I provides an overview of the organizations and simulation codes participating in the AN test simulation exercise, along with a summary of the key FGR-related features implemented in each code.

Table I. FGR-related features in the codes participating to the Simulation Exercise.

Participant	Code	Dimension	FGR model	Axial gas transfer model	Stress dependent gas swelling	Burst FGR
CEA	ALCYONE	1.5D, 3.5D	[15]	Yes	Yes	No
JAEA	FEMAXI	2DRZ	[16]	[17]	Yes	No
USNRC	FAST	1.5D	[18]	No	No	No
CIEMAT	FRAPCON	1.5D	[18]	No	No	No
SCK CEN	TRANSURANUS	1.5D	[11]	No	No	[10]
INL	BISON	2DRZ	[19]	No	No	[20]
Westinghouse	BISON	2DRZ	[19]	No	No	[20]

The CEA's ALCYONE-2.2.8 code employs the mechanistic CARACAS model for Fission Gas Release (FGR) [15]. Worth to mention is the macroscopic stress-dependency of gas bubble swelling that is available in this model. While CARACAS does not account for burst release, ALCYONE includes an axial gas transfer mechanism that can model delayed redistribution of released gases to the plenum. The JAEA's FEMAXI-8 code features a mechanistic FGR model [16] that also includes a stress-dependent gas bubble swelling. The axial gas transfer model [17] available in FEMAXI was not used in this SE. The USNRC's FAST-1.2 code, and its predecessor FRAPCON-4—used in this exercise by CIEMAT—are based on the Massih and Forsberg gas diffusion model [18], but do not incorporate burst release or axial gas transfer mechanisms. The BISON code, used by INL and Westinghouse, includes a burst release model [19][20], but lacks axial gas transfer capabilities. For TRANSURANUS, simulations performed at SCK CEN can utilize burst release models [8][10]. In this exercise, the burst FGR model developed by Pizzocri [11] is employed. The diversity of modeling approaches among the seven participating codes offers a valuable opportunity to independently assess the influence of stress-dependent fission gas bubble swelling, axial gas transfer and burst release on pressure and FGR evolution during the AN3 and AN10 tests. It is worth noting that AN3 has already been simulated using the BISON, TRANSURANUS and FRACON codes [11][13], and other tests from the AN series are part of the FAST validation database. However, AN10 represents a new case for all participating codes.

4. RESULTS AND DISCUSSION

The presentation of results will focus primarily on the bump tests. Prior to this, all participating codes were required to simulate the four irradiation cycles in the Biblis A PWR that preceded the tests. Overall, the

results at the end of the base irradiation showed a reasonable spread across codes, which is not expected to significantly influence the predicted behavior during the bump tests. In particular, the low Fission Gas Release (FGR) of 0.2% observed during base irradiation suggests minimal impact on the calculation of rod internal pressure increase during the subsequent ramp tests. Furthermore, the accurate estimation of average burnup across the codes indicates that the fission gas inventory prior to the bump tests should be consistent. Additionally, the segment free volume at the end of base irradiation was verified against experimental measurements, with deviations remaining within 20%.

Figure 2 shows the calculated and measured temperature evolutions at the thermocouple axial location during the AN3 and AN10 bump tests.

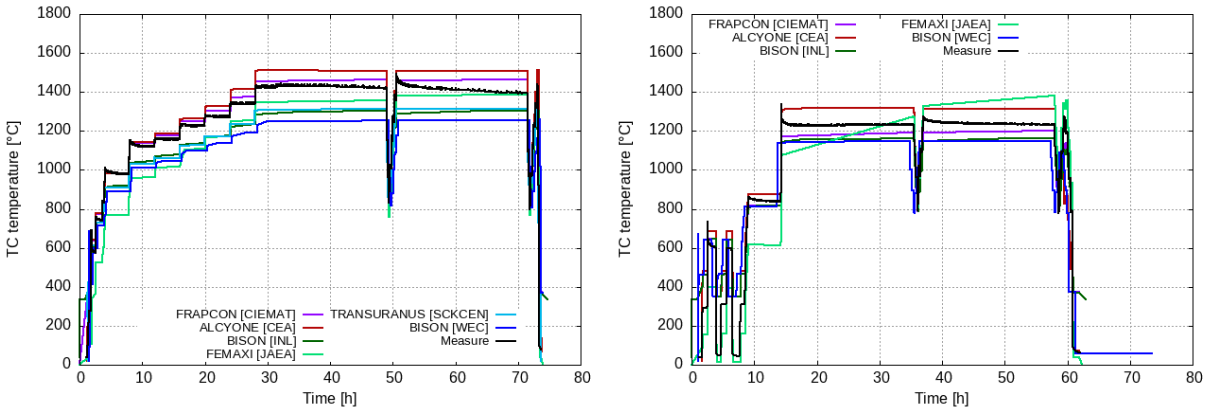

Figure 2. Calculated and measured temperature evolutions at the thermocouple axial location during the AN3 (left) and AN10 (right) bump tests.

Overall, the codes successfully capture the stepwise temperature increase observed during the bump tests. However, there is a variation of up to 300°C in the predicted maximum temperatures at peak Linear Heat Rate (LHR). All codes show either constant or slightly increasing temperatures during the LHR plateaus, but none are able to reproduce the initial temperature drop observed in the experimental data at the beginning of these plateaus (see, for example, the AN3 plot around 50 hours in Figure 2). This discrepancy has recently been attributed by Khvostov [14] to a possible axial displacement of the thermocouple within the central hole. An alternative explanation lies in the well-documented improvement in fuel thermal conductivity at high temperatures [21], which is associated with the annealing of irradiation-induced defects.

Figure 3 presents the calculated temperature evolutions at the pellet centerline (PPN) during the AN3 and AN10 bump tests. The scatter in predicted maximum temperatures at the PPN is comparable to that observed at the thermocouple location, with variations of up to 300°C. For AN3, the maximum calculated temperature reaches approximately 2000°C, while for AN10 it is around 1800°C. Interestingly, FAST predicts nearly identical peak temperatures for both bump tests, despite the clear difference in maximum Linear Heat Rate (LHR). In contrast, other codes yield a temperature difference of about 200°C between AN3 and AN10, more in line with expectations based on the LHR variation. It is important to note that the external cladding temperatures were prescribed in the simulations, using correlations provided in the AN3 [22] and AN10 [23] reports. As a result, differences in fuel pellet central temperatures cannot be attributed to discrepancies in cladding surface temperature predictions across the codes.

Figure 4 shows the calculated and measured plenum pressure evolutions during the AN3 bump test. The general trend of increasing plenum pressure—driven by both the reduction in free volume and the rise in plenum temperature—is captured by all the codes, although with varying slopes. These differences arise primarily from variations in the calculated fuel pellet–cladding gap before the bump test and from the choice

of temperature used for the plenum gas (e.g., external cladding temperature, internal cladding temperature, fuel average temperature, or a combination of these).

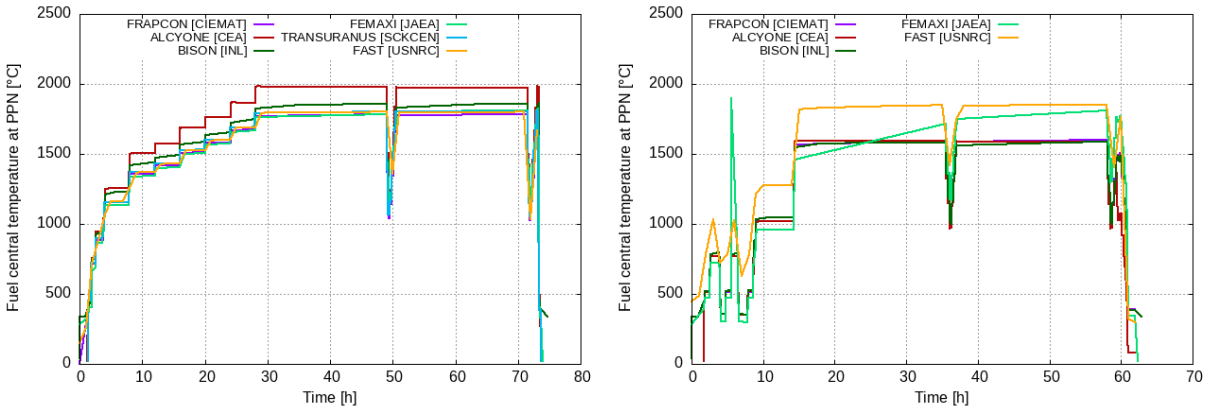

Figure 3. Calculated and measured temperature evolutions at the Peak Power Node axial location during the AN3 (left) and AN10 (right) bump tests.

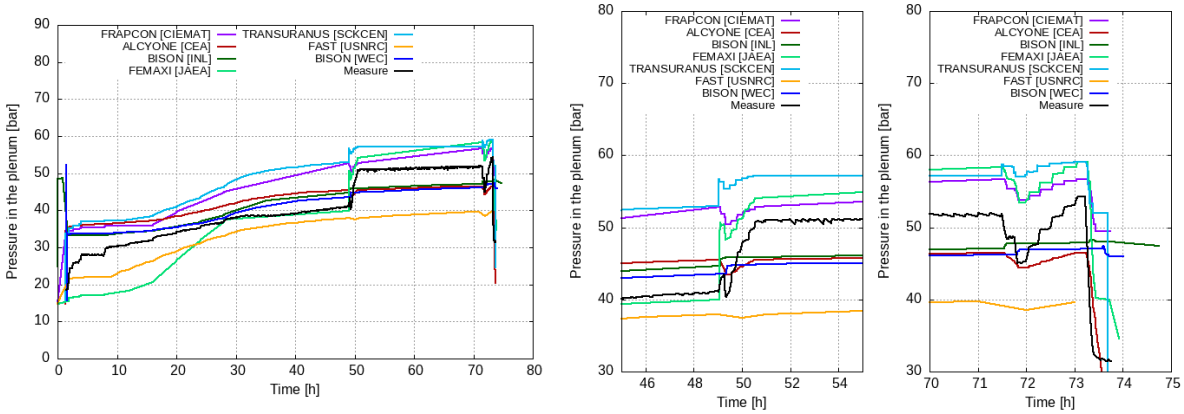

Figure 4. Calculated and measured plenum pressure evolutions during the AN3 bump test (zoom on the two power dips in the graphs on the right).

During the power dips, the codes that lack a burst release or axial gas transfer model (such as FRAPCON and FAST) predict a pressure drop, mainly due to the increase in free volume associated with the reopening of the fuel–clad gap. In contrast, FEMAXI, which incorporates a stress-dependent fission gas bubble swelling model, reproduces both the shape and magnitude of the pressure variations during the two dips. Specifically, it predicts a 10-bar increase in pressure during the first dip. During the second dip, pressure initially decreases by 7–8 bar and then rises again by approximately 10 bar.

ALCYONE, which also includes a stress-dependent fission gas bubble swelling model, does not predict any pressure increase during the dips. This behavior can be attributed to the absence of gap reopening, consistent with the very small residual gap (8 μm) calculated at the end of base irradiation—the smallest among all codes. In consequence, the stress level remains high in the pellet and hinders FGR. BISON, which includes a burst FGR model, predicts a modest plenum pressure increase of around 1 bar during the power dips. The TRANSURANUS code, which uses the same burst release model but a different overall FGR model, shows a more pronounced pressure increase of 4–5 bar during the first dip.

Figure 5 presents the calculated and measured plenum pressure evolutions during the AN10 bump test. The simulation results follow trends similar to those observed for AN3. Notably, none of the codes reproduce the 6-bar pressure increase observed during the first power dip. Both BISON and FEMAXI predict only a 1-bar pressure increase, which may be attributed to the lower amount of fission gas available at grain boundaries in AN10 compared to AN3—likely a consequence of the lower Linear Heat Rate (LHR). The 3-bar pressure increase observed during the second power dip is, however, well captured by FEMAXI. That said, the code significantly overestimates the pressure evolution during the LHR plateau preceding this dip. ALCYONE, which employs a similar gas model, does not predict any pressure increase during the dips, consistent with its behavior in AN3 and due to the lack of gap reopening resulting from a minimal residual gap. BISON's burst FGR model predicts a small pressure increase—less than 1 bar—during the second power dip, in line with the lower FGR expected under AN10's milder thermal conditions.

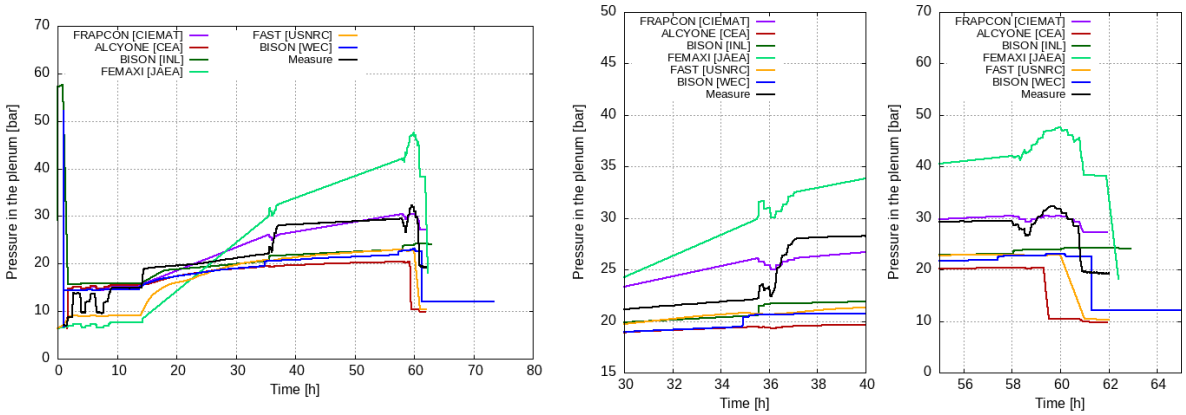

Figure 5. Calculated and measured plenum pressure evolutions during the AN10 bump test (zoom on the two power dips in the graphs on the right).

Figure 6 presents plots of the calculated and estimated FGR (from the measured plenum pressure) evolutions during the AN3 and AN10 bump test.

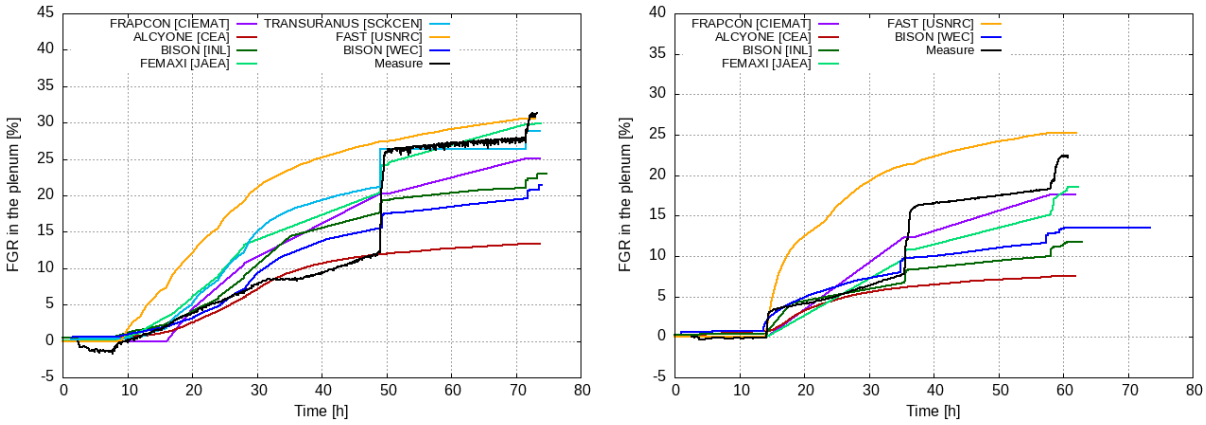

Figure 6. Calculated and estimated FGR evolutions during the AN3 (left) and AN10 (right) bump tests.

It is important to note that the "measured FGR" values during the bump tests are not direct measurements but are estimated from plenum pressure data. This estimation involves applying LHR-dependent correction

factors to convert hot pressure measurements to their cold equivalents, from which the initial cold pressures are subtracted [22][23]. Additionally, the free volume is assumed to remain constant throughout the bump tests when estimating FGR. These correction factors are test-specific, introducing multiple sources of uncertainty in the comparison between calculated and estimated FGR values. A further limitation arises in the case of AN3, where no final FGR measurement via rod puncturing was performed. As a result, there is no direct validation of the pressure-based FGR estimation for this test. In contrast, for AN10, rod puncturing was carried out at the end of the test, providing reliable measurements of the final pressure, free volume, and FGR. These experimentally obtained values are compared to the code predictions in Figure 7.

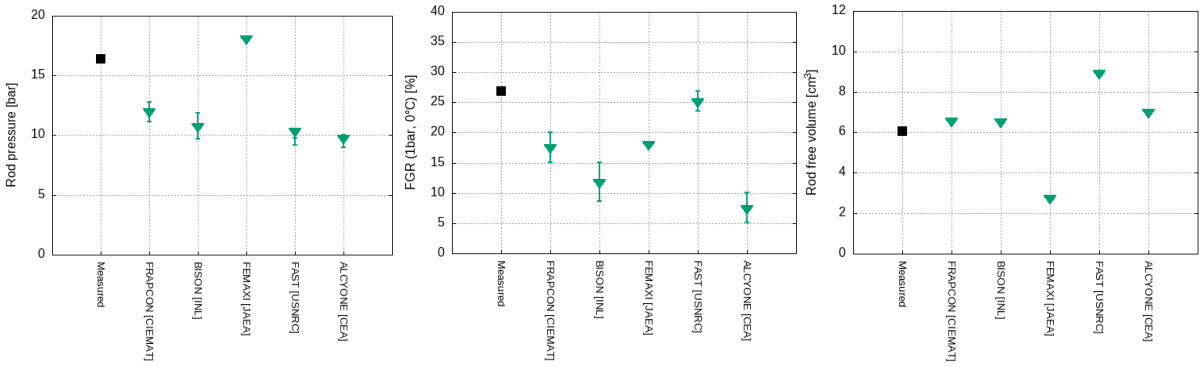

Figure 7. Calculated and measured rod pressure (left), FGR (center) and rod free volume (right) at the end of the AN10 bump test.

The FGR measured by rod puncturing at the end of the AN10 bump test is 26.9%, in reasonable agreement with the 22.5% estimated from pressure measurements. The FAST and FRAPCON codes produce consistent estimates of the final FGRs but fail to accurately reproduce the time evolution of FGR, particularly during the LHR plateaus and power dips. ALCYONE shows good agreement with the estimated FGR evolution during the LHR plateaus; however, it does not capture the FGR steps observed during power dips, resulting in a significant underestimation of the total FGR at the end of the test. Similarly, the sharp FGR increases during the first power dips—approximately 15% for AN3 and 10% for AN10—are not well reproduced by FEMAXI, BISON, or TRANSURANUS, despite the presence of stress-dependent fission gas bubble swelling and burst FGR models in these codes. All these codes underestimate the magnitude of the FGR jumps, in line with their underprediction of the associated pressure increases. Variations in the assumed plenum temperatures and segment free volumes during power dips may contribute to the difficulty in accurately capturing these FGR and pressure transients.

The left graph of Figure 7 shows that all codes underestimate the final segment pressure (16.4 bar) by approximately 50%, with the exception of FEMAXI, which predicts a final pressure of 18 bar. However, FEMAXI significantly overestimates the pressure throughout the AN10 test, as previously shown in Figure 5. This apparent agreement with the final pressure is due to an underestimated free volume (2.6 cm^3 compared to the measured 6 cm^3), as illustrated in the right graph of Figure 7. In contrast, the other codes provide more accurate estimates of the segment's free volume, and their underestimation of the final pressure is primarily linked to an underprediction of FGR during the test. These results highlight the critical value of rod puncturing at the end of tests with online pressure measurements—such as the upcoming P2M-Q1 experiment—to validate and interpret code predictions, particularly regarding FGR and internal pressure evolution.

Figure 8 presents the calculated and measured xenon distributions in the fuel pellet—obtained via X-ray fluorescence—at three different axial locations after the AN3 bump test. These measurements are particularly useful in determining whether the underestimation of segment FGR arises uniformly across the segment or is more pronounced in the end regions exposed to lower LHRs. As shown in Figure 8, all

codes—including ALCYONE, which significantly underpredicts the total segment FGR—provide reasonably accurate estimates of the radial Xe profiles near the PPN (at 193 mm and 214 mm), where the LHR peaked at 415 W/cm. However, at 265 mm, where the LHR was lower (365 W/cm), all codes overestimate the amount of Xe retained in the fuel, with the exception of TRANSURANUS, which predicts a radial profile nearly identical to those at the higher LHR locations. According to the AN3 report, the estimated FGR at 193 mm and 214 mm was 34%, while it dropped to 25% at 265 mm. These findings suggest that the underestimation of the total segment FGR may stem from the temperature dependence embedded in the fission gas release models, which may not be sufficiently sensitive to moderate reductions in LHR. This is consistent with the more pronounced underestimation observed in AN10, which had an even lower maximum average LHR of 344 W/cm.

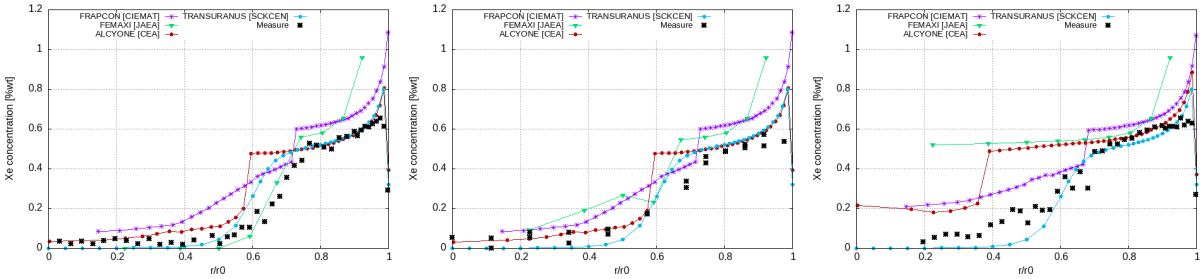

Figure 8. Calculated and measured distributions of Xe in the fuel pellet after the AN3 bump test at 193 mm (LHR 413 W/cm), 214 mm (415 W/cm) and 265 mm (365 W/cm) from the bottom of the fuel column.

5. 3.5D SIMULATIONS

The reopening of the pellet–clad gap during power dips is a critical mechanism for accurately predicting plenum pressure increases when axial gas transfer models are employed in simulations. In the case of ALCYONE, simulations of both AN3 and AN10 failed to capture this behavior, as the gap remained closed throughout the power dips. To assess the validity of this outcome, an additional simulation of the AN3 bump test was conducted using ALCYONE's 3.5D scheme [4]. This scheme shares the same physical models as the 1.5D version but enhances spatial resolution by performing 3D calculations of the fragmented fuel pellet and surrounding cladding at each axial slice. This approach enables a more accurate representation of pellet geometry—including features such as the dish and chamfer—and allows for a more realistic assessment of gap reopening and free volume evolution. Figure 9 presents the calculated temperature distribution and fuel pellet deformation from the 3.5D simulation of AN3, shown at two time points: (1) at the maximum LHR just before the first power dip, and (2) at the minimum LHR during the dip.

The pellet–clad contact conditions shown in the top panel of Figure 9 are characteristic of the mechanical state during a power ramp. The gap is fully closed along the entire height of the segment. At this stage, the radial cracks in the fuel pellets—formed during base irradiation—are open at their tips, inducing localized strain and stress concentrations in the cladding [24]. These stress concentrations are known contributors to failures by Iodine Stress Corrosion Cracking (I-SCC). During the power dip (Figure 9, bottom), some reopening of the gap is observed at pellet–pellet interfaces (IP). However, the gap remains closed at the mid-pellet level (MP), due to the continued effect of fission gas swelling, which is more pronounced in the central region of the fuel pellet. Because the 1.5D simulations capture only the mid-pellet behavior, the 3.5D results confirm that axial gas migration remains hindered during the power dip. It is worth noting that the segment pressure and FGR evolutions predicted by the 3.5D simulation were very similar to those obtained with the 1.5D scheme, further validating the observed absence of significant axial gas transfer during the dip.

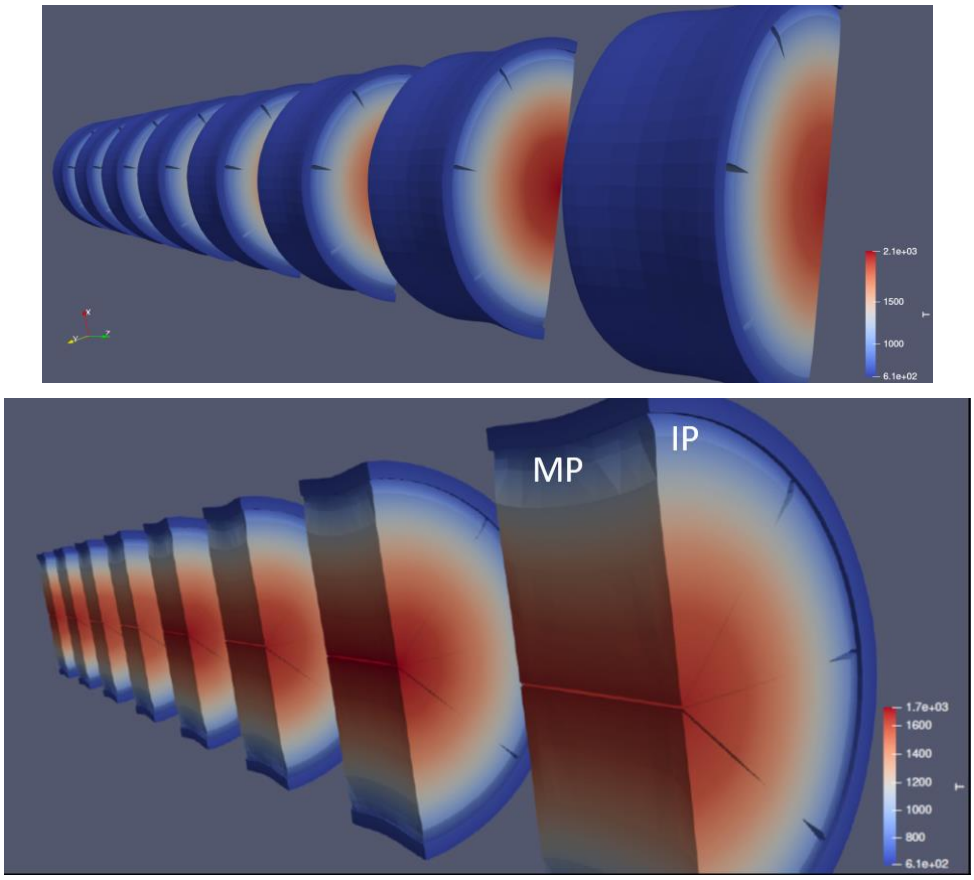

Figure 9. Calculated temperatures and deformation of the fuel pellets from the 3.5 simulation of AN3 with ALCYONE at two time points: (1) at the maximum LHR just before the first power dip (top), and (2) at the minimum LHR during the dip (bottom).

6. CONCLUSIONS

This paper has presented the main outcomes of the FIDES-II/P2M Simulation Exercise focused on the AN3 and AN10 bump tests. The participation of multiple institutions using a diverse set of fuel performance codes enabled a robust comparison of results obtained with: (i) advanced mechanistic fission gas release (FGR) models—with and without burst release, (ii) axial gas migration models, and (iii) refined free volume estimations through 3.5D simulations. While the 3.5D approach provided a more realistic representation of the fuel geometry, it did not significantly improve predictions of FGR or segment pressure compared to 1.5D simulations. In contrast, the stress-dependent fission gas bubble swelling model implemented in FEMAXI reproduced the pressure and FGR evolutions during power dips with reasonable accuracy. Burst release models in BISON and TRANSURANUS led to modest increases in pressure and FGR during the power dips but still fell short of matching the measured values. A key takeaway from this Simulation Exercise is the critical importance of rod puncturing at the end of irradiation in the upcoming P2M-Q1 test. Such direct measurements will be essential to validate and interpret the online pressure data and better constrain the models involved in simulating fission gas behavior under transient conditions.

ACKNOWLEDGMENTS

Dr. Martin Dostal from ÚJV Řež, Czechia, and Grigori Khvostov from PSI, Switzerland, are gratefully acknowledged for fruitful discussions on the AN experiments.

REFERENCES

[1] M. Bales, et al. (2024). The NEA Second Framework for irradiation experiments (FIDES-II): A proven, flexible platform for fuel and material research, TopFuel conference, Grenoble, France.

[2] D'Ambrosi, V., et al. (2024). P2M Simulation Exercise on Past Fuel Melting Irradiation Experiments, Nuclear Technology 210.2, 189-215.

[3] Bosch, Rik-Wouter, et al. (2024). Development of Instrumented Fuel Pin Testing in the BR2 Reactor for the P2M Project, JOM 1-10.

[4] Introïni, C., et al. (2024). ALCYONE: the fuel performance code of the PLEIADES platform dedicated to PWR fuel rods behavior, Annals of Nuclear Energy, 207, 110711.

[5] Rozzia, D., et al. (2024). Modeling of OECD/NEA P2M Benchmark Cases by Means of TRANSURANUS Code, Nuclear Technology 210.2: 324-353.

[6] Chaieb, A., et al. (2024). Modeling of the P2M Past Fuel Melting Experiments with the Fuel Performance Code CYRANO3, Nuclear Technology 210.2: 232-244.

[7] Turnbull, J. A. (1995). IFPE/RISOE-III, Fuel Performance Data from 3. Risoe Fission Gas Release.

[8] Koo, Y.-H. et al. (1999). COSMOS: a computer code to analyze LWR UO2 and MOX fuel up to high burnup, Annals of Nuclear Energy 26.1: 47-67.

[9] Fuel Modelling at Extended Burnup (FUMEX-II), (2012). IAEA-TECDOC-1687.

[10] Pizzocri D., et al. (2015). Modelling of Burst Release in Oxide Fuel and Application to the Transuranus Code, 11th International Conference on WWER Fuel Performance, Varna, Bulgaria.

[11] Barani, T., et al. (2017). Analysis of transient fission gas behaviour in oxide fuel using BISON and TRANSURANUS, Journal of Nuclear Materials 486: 96-110.

[12] Scolaro, A. et al. (2022). Towards coupling conventional with high-fidelity fuel behavior analysis tools, Progress in Nuclear Energy, 152, 104357.

[13] Pizzocri, D. et al. (2025). A multi-fidelity multi-scale methodology to accelerate development of fuel performance codes, Nuclear Engineering and Design 432: 113741.

[14] Khvostov, G. (2024). Interpretation of the online measurement data for selected tests of the RISOE-III project, Journal of Nuclear Materials 599:155219.

[15] Jomard, G. et al. (2014). CARACAS, An industrial model for the description of fission gas behavior in LWR-UO_2 fuel, TopFuel conference, Sendai, Japan.

[16] Udagawa, Y. et al. (2019). Model updates and performance evaluations on fuel performance code FEMAXI-8 for light water reactor fuel analysis, Journal of Nuclear Science and Technology 56.6: 461-470.

[17] Taniguchi, Y. et al. (2024). High-temperature rupture failure of high-burnup LWR-MOX fuel under a reactivity-initiated accident condition, Annals of Nuclear Energy 195: 110144.

[18] Forsberg, K., and A. R. Massih (1985). Diffusion theory of fission gas migration in irradiated nuclear fuel UO2, Journal of nuclear materials, 135.2-3: 140-148.

[19] Pastore, G., et al. (2013). Physics-based modelling of fission gas swelling and release in UO2 applied to integral fuel rod analysis, Nuclear Engineering and Design 256: 75-86.

[20] Pastore, G., et al. (2014). Modelling of transient fission gas behaviour in oxide fuel and application to the BISON code, Enlarged Halden Programme Group Meeting, Røros, Norway.

[21] Bouloré, A., et al. (2023). Modelling of UO_2 thermal conductivity: Improvement of the irradiation defects contribution and uncertainty quantification, Nuclear Engineering and Design 407: 112304.

[22] Bump Test AN3 (CB8-2R), Risø-FGP3-AN3 report, September 1990, available in the IFPE database.

[23] Bump Test AN10 (CB13-4R), Risø-FGP3-AN10 report, September 1990, available in the IFPE database.

[24] Sercombe, J., et al. (2020). Modeling of Pellet Cladding Interaction, Comprehensive Nuclear Materials-Second Edition. Volume 2: Oxide Fuel Systems in Thermal and Fast Neutron Spectrum Reactors 2.2.14.